# Adaptive Array Radar Imaging of a Human Body for Vital Sign Measurement

Takuya Sakamoto*, Kentaro Konishi, Kosuke Yamashita, Masashi Muragaki, Shigeaki Okumura, and Toru Sato
Graduate School of Engineering, University of Hyogo
2167 Shosha, 671-2280 Himeji, Japan
Graduate School of Informatics, Kyoto University
Yoshida-Honmachi, Sakyo-ku, 606-8501 Kyoto, Japan

***Abstract*—This study demonstrates the feasibility of human body imaging using an array radar system for monitoring vital signs. In this study, a depth camera is used to obtain a numerical three-dimensional model of a human body, which is used for electromagnetic scattering simulation. We apply physical optics approximation for numerical analysis, and the simulated radar echoes are processed to find the position of the scattering centers on the human body.**

## I. Introduction

Measurement of vital signs in non-medical settings is currently attracting substantial attention, as exemplified by the rise of smartwatches, such as the Apple Watch (Apple Inc. Cupertino, CA, USA). Radar-based remote measurement of vital signs is emerging as a new technology, and is expected to play an important role in various applications such as healthcare and nursing [1]. Using microwave or mm-wave, measurements can be performed non-invasively without electrodes or wearable devices attached to the skin [2], [3]. Thus, the target individual might not be even aware of the measurement itself. Monitoring heart rate is important, particularly during sleep, because many cardiovascular symptoms are caused by increased heart rate during rapid eye moving (REM) sleep. Previous studies report that the accuracy of heart rate measurement during sleep is strongly affected by the orientation and posture of the target person. Nonetheless, the factors determining the accuracy of remote measurement of heart rate remain unclear. In this paper, we describe a feasibility study using array-radar imaging of a sleeping human body for finding the reflection points, which is crucial for realizing accurate measurement of vital signs. In this study, a depth camera is used to obtain a three-dimensional human body shape, which is used for numerical electromagnetic scattering analysis.

## II. Measurement of Human Body Shape Using Depth Camera

A depth camera (Kinect version 2; Microsoft Corporation, Redmond, WA, USA) is used for recording a participant while lying down 1.5 m from the camera. The depth image size is $512 \times 424$ pixels, the frame rate is 30 fps, accuracy is $\pm$ 3 mm, and the horizontal and vertical field of vision are $\pm 35^\circ$ and $\pm 30^\circ$, respectively. Figure 1 shows a depth image recorded using the depth camera. From the recorded depth image, we calculate the normal vector $\boldsymbol{n}$. The angle $\psi$ between the normal vector $\boldsymbol{n}$ and the line-of-sight direction $\boldsymbol{r}$ is calculated, and its cosine $|\cos\psi|$ is shown in Fig. 2. The geometrical optics approximation detects pixels with a value of one in Fig. 2 to locate the reflection points. This method instead adopts the physical optics for estimating more accurate scattering echoes as introduced by Muragaki *et al.* [4], which will be described in the folloiwng section.

## III. Electromagnetic Scattering Analysis Using Physical Optics Approximation

We assume a non-modulated radar system with an operating frequency of 60.0 GHz. The transmitting and receiving antennas are closely located, forming a quasi-monostatic configuration. The transmitting antenna is modeled as a short dipole antenna in the $z$-direction located at the origin $\boldsymbol{r}_\mathrm{T} = \boldsymbol{0}$. The azimuth component $H_\phi$ of the radiated magnetic field at position $\boldsymbol{r}$ is

$$H_\phi(\boldsymbol{r}) = \frac{Il}{4\pi}\left(\mathrm{j}\frac{k}{r} + \frac{1}{r^2}\right)\sin\theta \mathrm{e}^{-\mathrm{j}kr}, \qquad (1)$$

where $r = |\boldsymbol{r}|$, $\theta$ is an elevation angle, $I$ and $l$ are the current and length of the antenna, respectively, and $k = 2\pi/\lambda$ is the wavenumber corresponding to wavelength $\lambda$. The other components of the magnetic field are zero: $H_r = H_\theta = 0$.

We model the material of the human body surface as a perfect electric conductor (PEC) for simplicity, which provides a good approximation at a higher frequency. In physical optics, the induced current density on the PEC surface is approximated as $\boldsymbol{i} = 2\boldsymbol{n} \times \boldsymbol{H}$, where $\boldsymbol{n}$ is the normal vector, and $\boldsymbol{H}$ is the magnetic field radiated from the short dipole antenna.

The receiving antenna is also vertically polarized and located at $\boldsymbol{r}_\mathrm{R}$. We calculate $E_z^\mathrm{rec}(\boldsymbol{r}_\mathrm{R})$, which is the $z$-component of the electric field at $\boldsymbol{r}_\mathrm{R}$, radiated from the induced current. The total electric field at the receiving antenna position is obtained by integrating $\hat{E}_z(\boldsymbol{r}_\mathrm{R}, \boldsymbol{r})$, which is the $z$-component of the scattered electric field due to the current at $\boldsymbol{r}$, as

$$E_z^\mathrm{rec}(\boldsymbol{r}_\mathrm{R}) = \iint_{S_0} \hat{E}_z(\boldsymbol{r}_\mathrm{R}, \boldsymbol{r})\mathrm{d}S, \qquad (2)$$

where $S_0$ is the entire body surface measured using the depth camera, and $\mathrm{d}S$ is a small area at $\boldsymbol{r}$.

To locate the position of the surface current contributing the received signal, we use a visualization technique proposed by

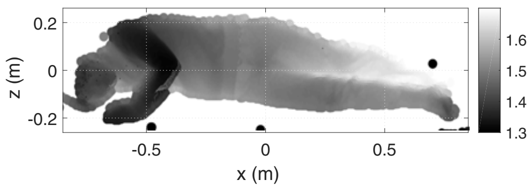


Fig. 1. Depth image recorded using the depth camera (in meters).

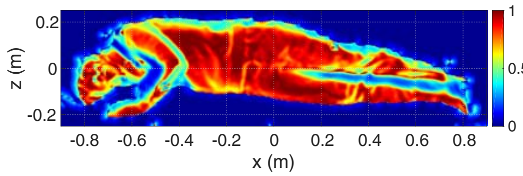


Fig. 2. Cosine of the angle between the normal vector and line-of-sight direction.

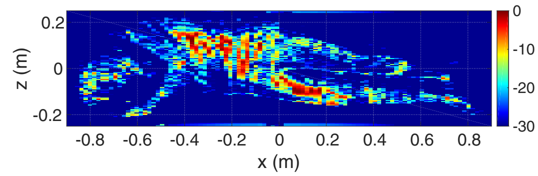


Fig. 3. Surface current contributing to the received radar echo calculated using the physical optics approximation (in decibels).

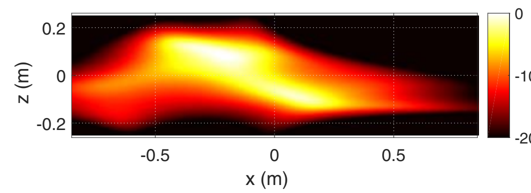


Fig. 4. Image generated using the Capon method from sixteen-channel radar echoes (in decibels).

Shijo *et al.* [5] using an eye function defined as

$$w(\boldsymbol{r}_0, \boldsymbol{r}) = \begin{cases} \frac{1}{2}(\cos(\pi|\boldsymbol{r}-\boldsymbol{r}_0|/a_0)+1) & (|\boldsymbol{r}-\boldsymbol{r}_0| \leq a_0) \\ 0 & (|\boldsymbol{r}-\boldsymbol{r}_0| > a_0), \end{cases} \tag{3}$$

where $a_0$ is the size of the eye function, and is set as $a_0 = 9$ mm in this study. Let $\hat{E}_z(\boldsymbol{r}_\mathrm{R}, \boldsymbol{r}_0)$ denote the $z$-component of the scattered electric field radiated from the current at $\boldsymbol{r}_0$ and measured at $\boldsymbol{r}_\mathrm{R}$. The contribution of a local surface current $E_z(\boldsymbol{r}_\mathrm{R}, \boldsymbol{r}_0)$ is calculated as

$$E_z(\boldsymbol{r}_\mathrm{R}, \boldsymbol{r}_0) = \iint_{S_0} w(\boldsymbol{r}_0, \boldsymbol{r})\hat{E}_z(\boldsymbol{r}_\mathrm{R}, \boldsymbol{r})\mathrm{d}S. \tag{4}$$

Figure 3 shows the $|\hat{E}_z(\boldsymbol{r}_\mathrm{R}, \boldsymbol{r}_0)|^2$ as a function of $\boldsymbol{r}_0$ for a receiving antenna located at the origin $\boldsymbol{r}_\mathrm{R} = \boldsymbol{0}$. In this case, we see strong reflections from the left side of the torso, as well as the right thigh of the target person.

## IV. Adaptive Array Imaging

We simulate multi-channel array radar signals using Eq. (2) assuming four transmitters and four receivers, which form a multiple-input multiple-output (MIMO) radar system with $(4 \times 4 = 16)$ channels. We apply an adaptive array processing technique to the radar echoes and generate an image of the target person. Figure 4 shows an image generated using the Capon method, which is a high-resolution adaptive array imaging algorithm. From Figs. 3 and 4, we see that the dominant components of the reflections are correctly imaged using the Capon method. The use of such images is expected to enable identification of the body part associated with the vital signs to be measured.

## V. Conclusion

In this paper, we demonstrated the feasibility of imaging a human body using a MIMO radar, assuming the application of vital sign measurement of a sleeping person. To demonstrate the feasibility of adaptive array imaging, we calculated the radar echoes using an electromagnetic scattering simulation with physical optics approximation. Our simulation method generates realistic radar echoes. In addition, using the visualization technique of electromagnetic scattering, we identified the body parts providing the dominant contribution to the received radar echo. High-resolution imaging using the Capon method was applied to the radar echo and an image similar to the effective surface current distribution was successfully obtained.


## Acknowledgment

This study was supported in part by JSPS KAKENHI Grant (No. 25249057, 15K18077, and 15KK0243) and the Kyoto University Center of Innovation (COI) Program.


## References


[1] T. Sakamoto, R. Imasaka, H. Taki, T. Sato, M. Yoshioka, K. Inoue, T. Fukuda, and H. Sakai, "Feature-based correlation and topological similarity for interbeat interval estimation using ultra-wideband radar," *IEEE Trans. Bio-med. Eng.,* vol. 63, no. 4, pp. 747–757, 2016.

[2] T. Sakamoto, R. Imasaka, H. Taki, T. Sato, M. Yoshioka, K. Inoue, T. Fukuda, and H. Sakai, "Accurate heartbeat monitoring using ultra-wideband radar," *IEICE Electronics Express,* vol. 12, no. 3, pp. 20141197, 2015.

[3] T. Sakamoto, S. Okumura, R. Imanishi, H. Taki, T. Sato, M. Yoshioka, K. Inoue, T. Fukuda, and H. Sakai, "Remote heartbeat monitoring from human soles using 60-GHz ultra-wideband radar," *IEICE Electronics Express,* vol. 12, no. 21, pp. 20150786, 2015.

[4] M. Muragaki, S. Okumura, K. Maehara, T. Sakamoto, M. Yoshioka,K. Inoue, T. Fukuda, H. Sakai, and T. Sato, "Non-contact respiration measurement using ultra-wideband array radar with adaptive beamforming technique for cancer radiotherapy," *Proc. 2016 International Symposium on Antennas and Propagation,* pp. 440–441, 2016.

[5] T. Shijo, T. Itoh, and M. Ando, "Visualization of high frequency diffraction based on physical optics," *IEICE Trans. Electron.*, vol. E87-C, no. 9, 2017.